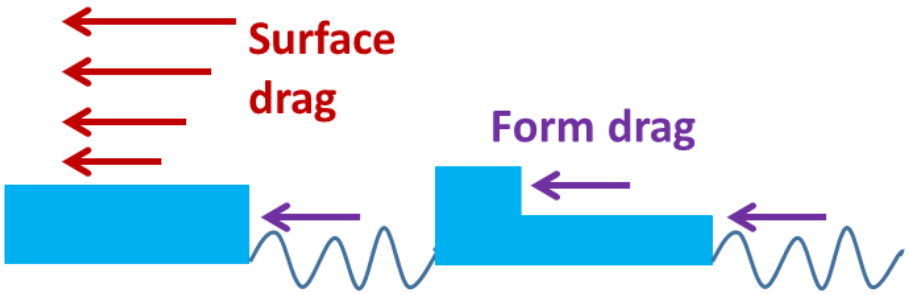

Figure 1 A sketch of the surface drag exerted on the atmosphere over the marginal ice zone, showing the surface (or skin) drag and the form drag caused by wind blowing against vertical faces.

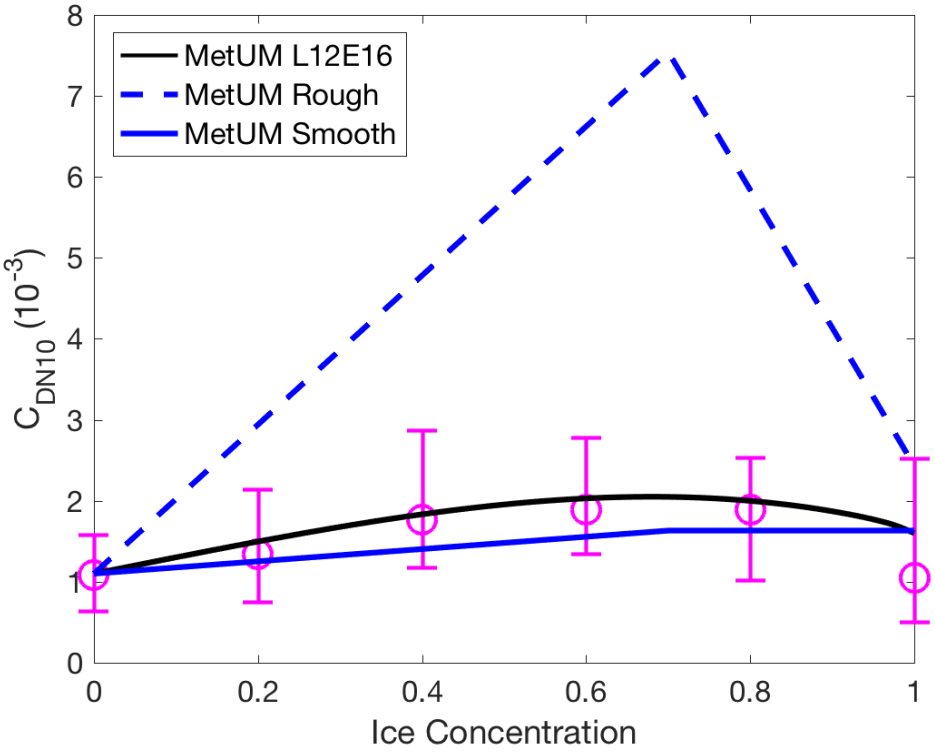

Figure 2 Neutral drag coefficient (C_{DN10}) as a function of ice concentration for the three parameterizations tested: the L12E16 scheme (following Lüpkes et al. 2012 and Elvidge et al. 2016) and the Rough and Smooth roughness lengths (see Table 1). Note C_{DNi} is set to 1.6×10^{-3}. Aircraft-based observations of C_{DN10} from Figure 2a of Elvidge et al. (2016) are shown as magenta circles (median) and whiskers (inter-quartile range).

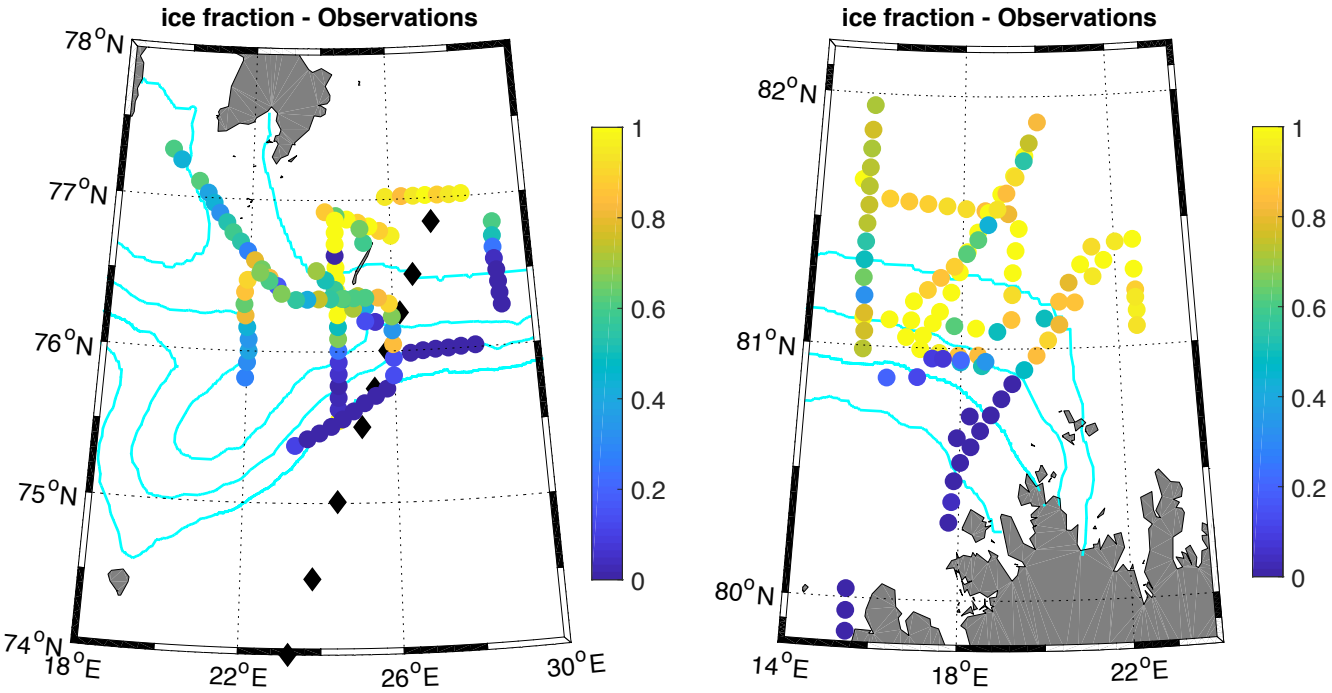

Figure 3 Compilation of ice fraction observations from the ACCACIA surface-layer data set (circles). This consists of 209 runs over 8 flights between 21 & 31 March 2013 – see Table 2 in Elvidge et al. (2016) for details. The data are shown here in two panels: to the south of Svalbard over the Barents Sea, and to the north of Svalbard over Fram Strait. Typical aircraft altitudes were around 35 m above sea level. Also shown are dropsonde locations (black diamonds) from flight B762 on 23 March 2013; and sea-ice fraction contours (from 0.2-0.8) from the OSTIA analysis.

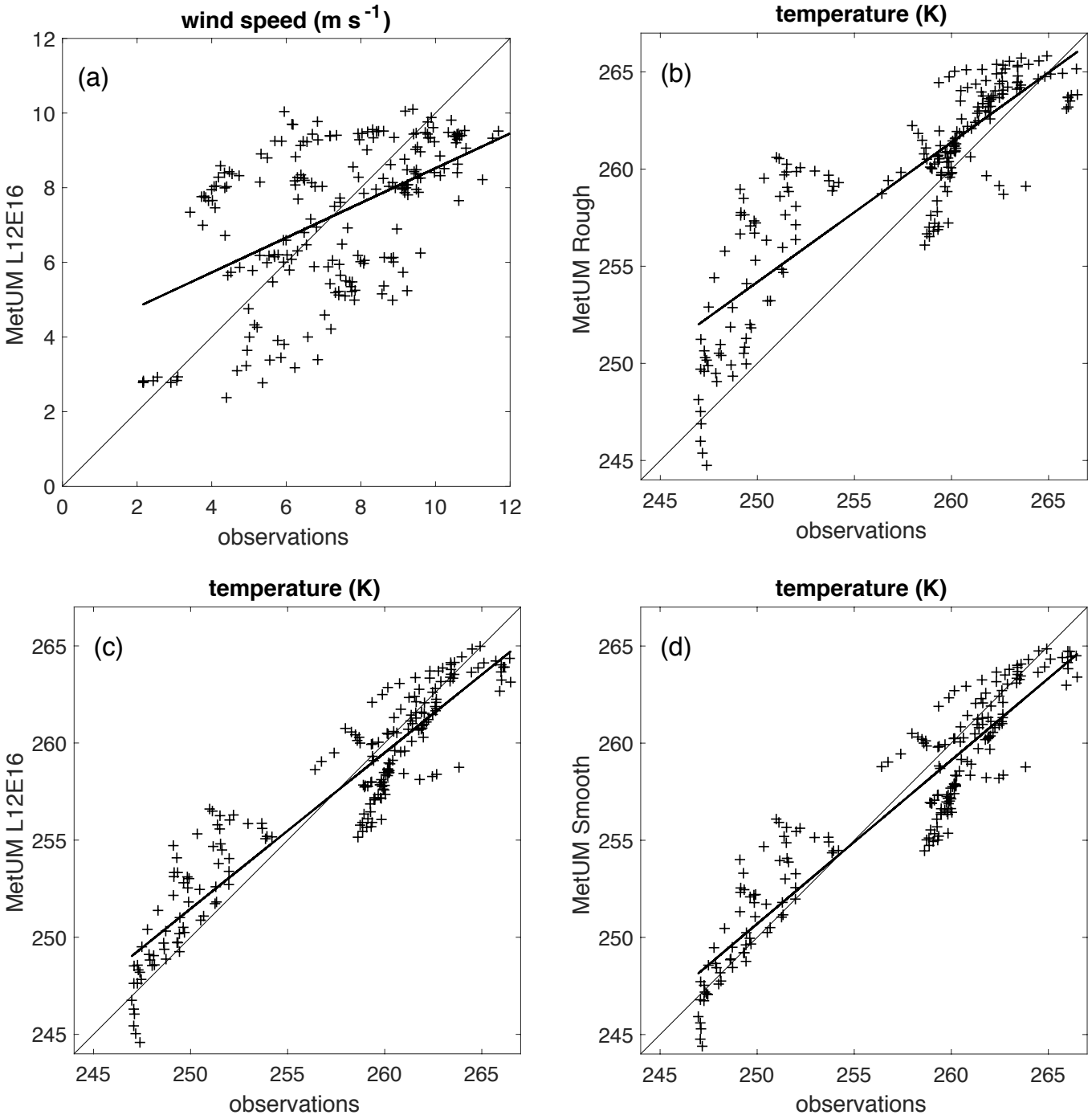

Figure 4 Scatter plot comparisons of flight-level aircraft observations against MetUM output for (a) wind speed for the L12E16 drag parameterization setting and (b)-(d) temperature for the (b) Rough, (c) L12E16 and (d) Smooth drag settings.

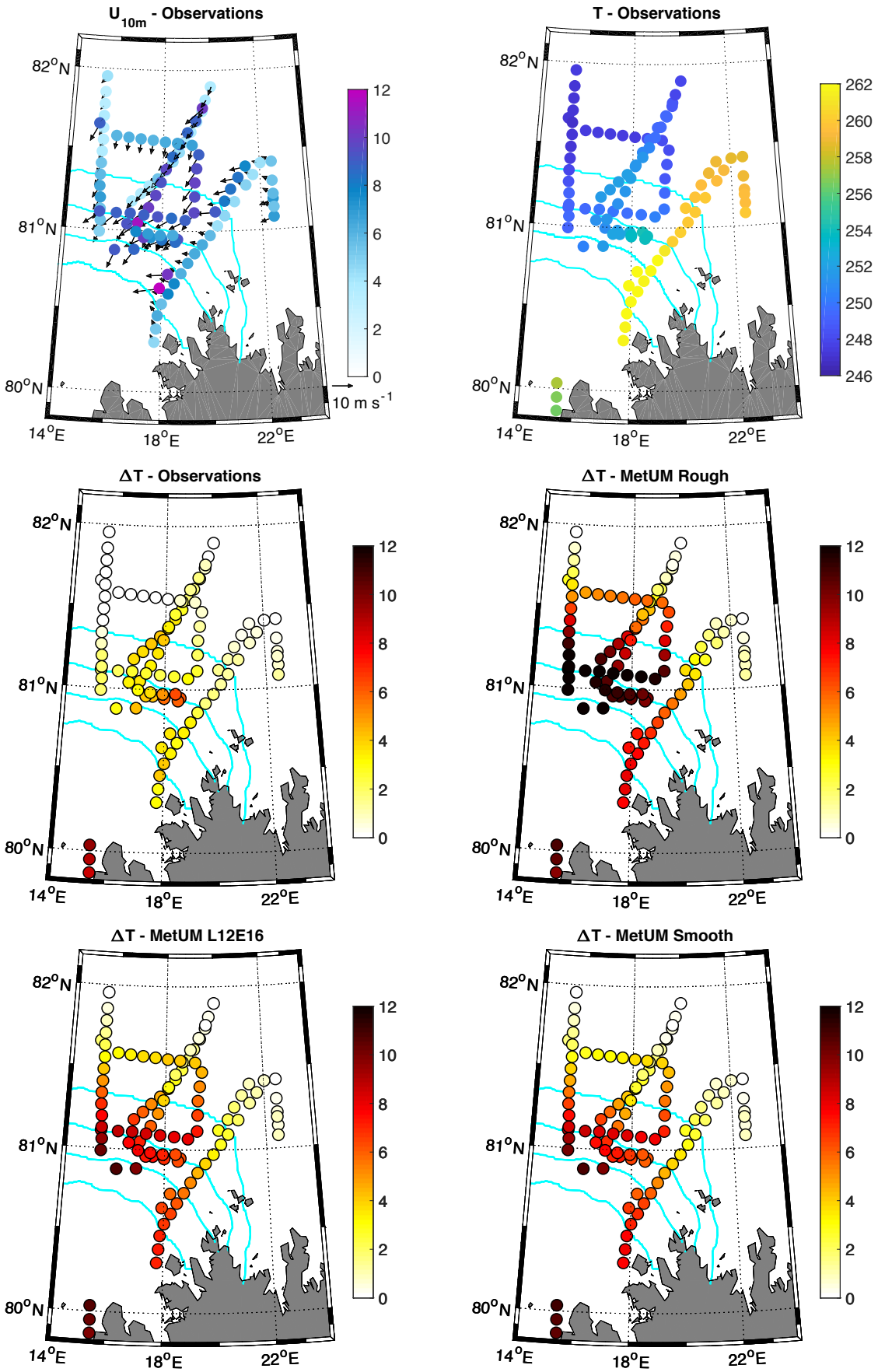

Figure 5 Surface-layer observations and model output for three flights to the north of Svalbard on 25, 26 and 29 March 2013. Panels show observations of (a) wind speed at 10 m, (b) temperature, and (c) temperature change (ΔT); as well as model output of ΔT from the surface drag experiments: (d) Rough, (e) L12E16, and (f) Smooth. The variable units are: m s^{-1} and K. Contours of ice fraction from the OSTIA analysis are also shown (from 0.2 to 0.8).

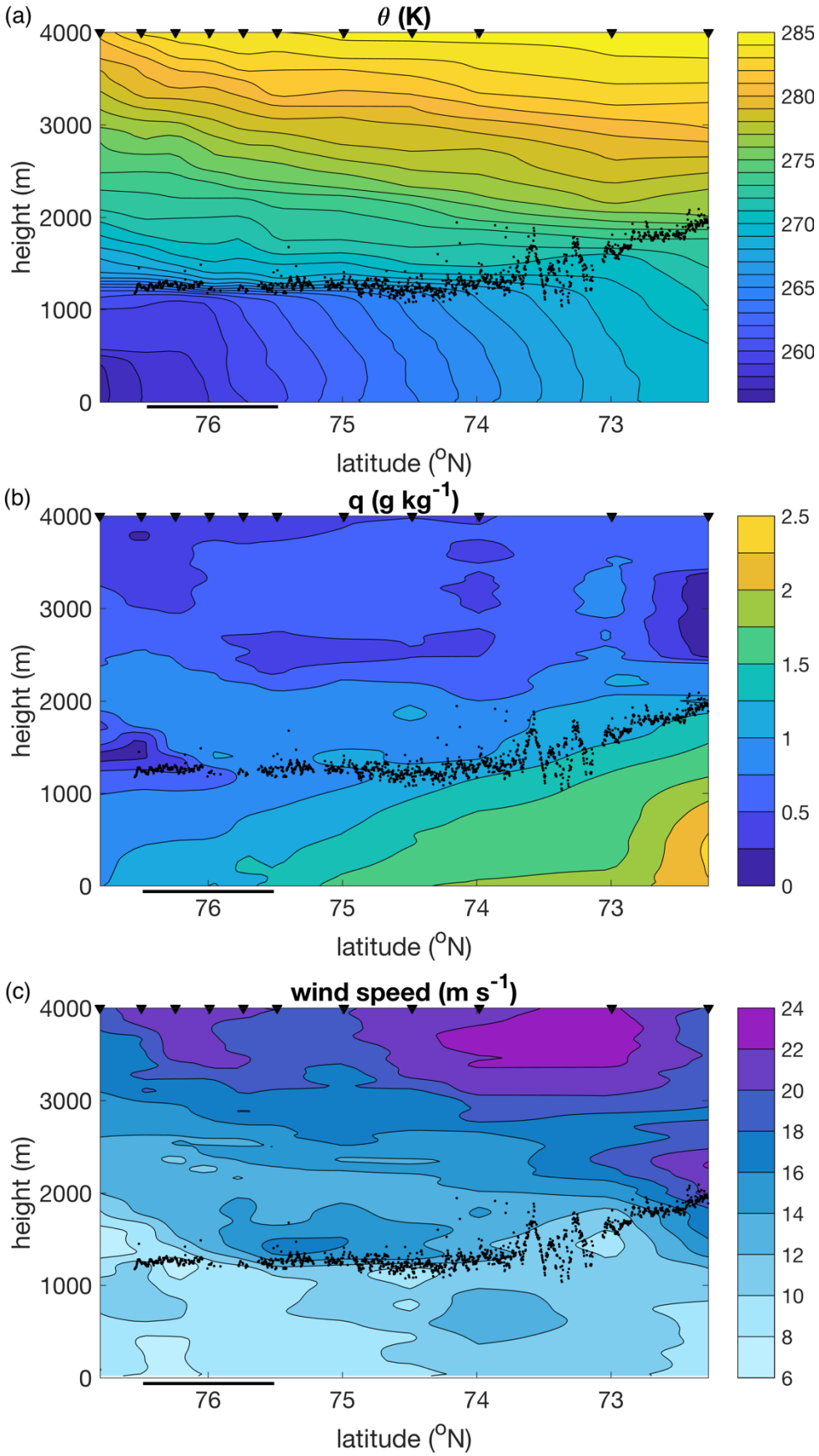

Figure 6 Cross-sections of (a) potential temperature (θ), (b) specific humidity (q) and (c) wind speed, from dropsonde data on 23 March 2013. Cloud top heights derived from airborne lidar observations are plotted as black dots. Note the winds are approximately from left to right and the MIZ is between ~76.5-75.5°N (thick black line). The cross-section is 530 km long. The black triangles mark the dropsonde release locations – see Fig. 3 for a location map of the northernmost 9 dropsondes.

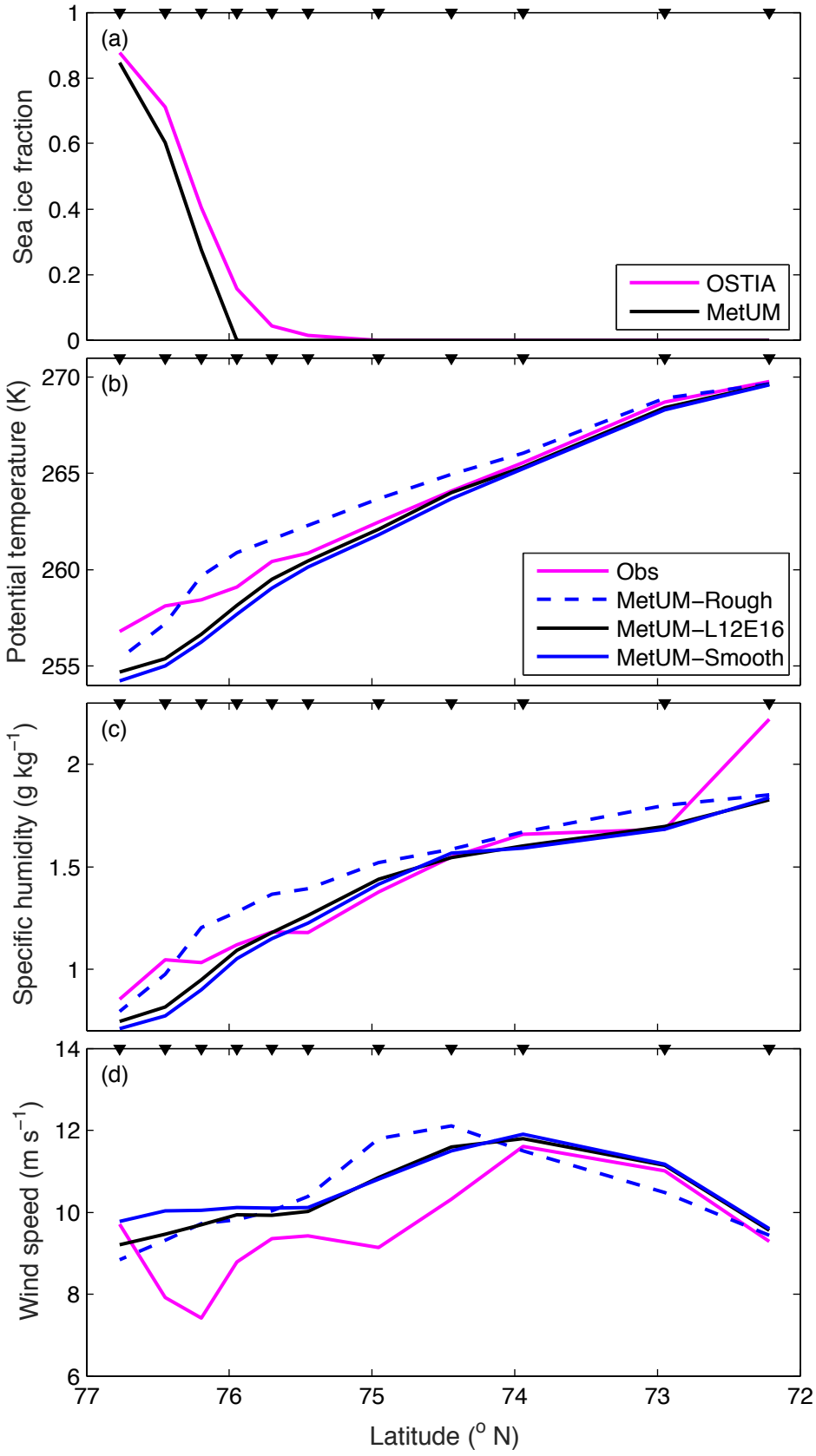

Figure 7 Observed and simulated variables from the dropsonde cross-section of 23 March 2013 shown in Fig. 6. Panel (a) shows sea-ice fraction from OSTIA and from the MetUM; the remaining panels are mixed-layer averages of (b) potential temperature, (c) specific humidity and (d) wind speed respectively. The black triangles mark dropsonde release locations (as in Fig. 6).

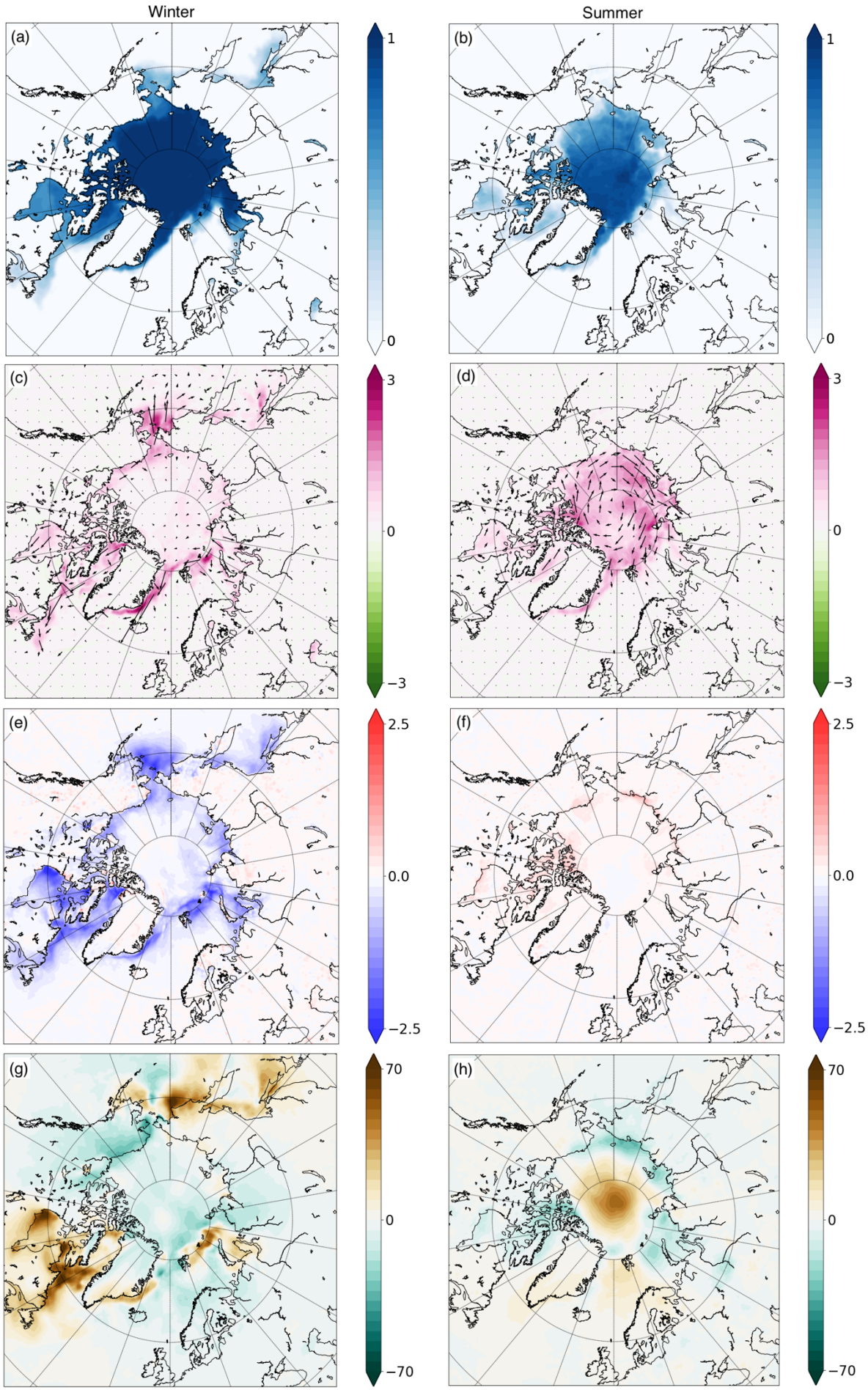

Figure 8 Composite global model output for the Northern Hemisphere showing (a, b) sea-ice fraction; and the difference between the MetUM L12E16 and Rough experiments for (c, d) wind speed, (e, f) near-surface temperature and (g, h) mean sea-level pressure. The left-hand panels are averaged over all extended winter cases (November-April); the right-hand panels are averaged over

all extended summer cases (May-October). The units for wind speed, temperature and pressure are m s^{-1}, K and Pa respectively.

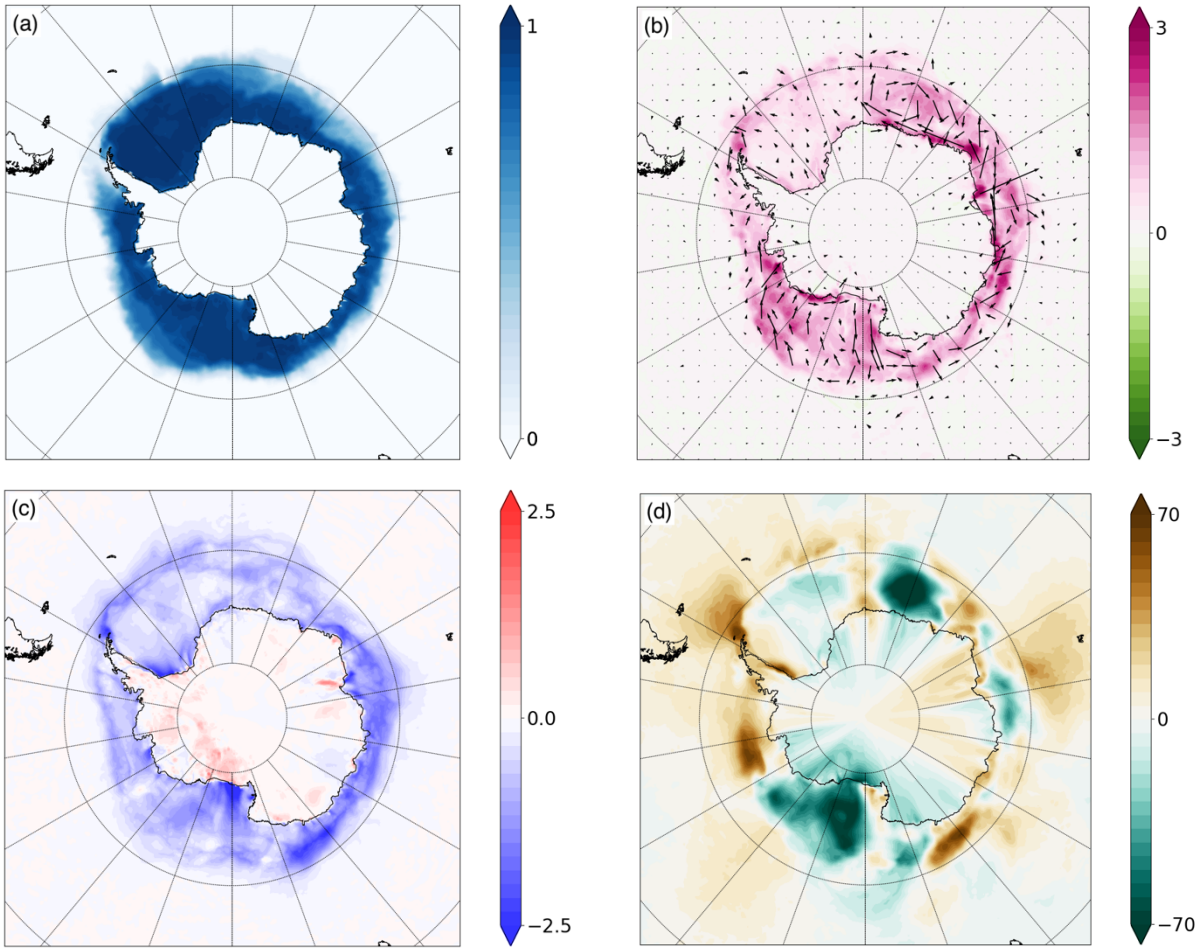

Figure 9 Composite global model output for the Southern Hemisphere showing (a) sea-ice fraction, and the difference between the MetUM L12E16 and Rough experiments for (b) wind speed, (c) near-surface temperature and (d) mean sea-level pressure, averaged over all extended winter cases (May-October). The units are the same as Fig. 8.